A characteristics study on the performance of a two-stage light gas gun

WU Yingxiang (吴应湘), ZHENG Zhichu (郑之初)

(Institute of Mechanics, Chinese Academy of Sciences, Beijing 100080, China)

and P. Kupschus

(JET Joint Undertaking, Oxon, England)

Received May 5, 1994

Abstract In order to obtain an overall and systematic understanding of the performance of a two-stage light gas gun (TLGG), a numerical code to simulate the process occurring in a gun shot is advanced based on the quasi-one-dimensional unsteady equations of motion with the real gas effect, friction and heat transfer taken into account in a characteristic formulation for both driver and propellant gas. Comparisons of projectile velocities and projectile pressures along the barrel with experimental results from JET (Joint European Torus) and with computational data got by the Lagrangian method indicate that this code can provide results with good accuracy over a wide range of gun geometry and loading conditions.

Keywords: two-stage light gas gun, method of characteristics, numerical simulation.

The first successful TLGG was manufactured in 1946 at the New Mexico School of Mines[1], since then it has been developed into a successful and powerful facility to study the aerodynamic physics of flight, high speed impacts and original ballistics. Recently, the great increase in propulsive velocity, the complexity of the designed projectile structure, the diversity of projectile materials (such as nonmetal material, fragile material, even deuterium and tritium ice pellets), and the wide usage of a TLGG (such as plasma fuel injector in tokamak fusion experiments, simulated equipment of vehicles proposed to fly at transonic, supersonic and hypersonic velocities), all acquire an overall and deep understanding of the behavior in its shooting process over a wide range of loading conditions and gun geometry.

There are two approaches to evaluating the performance of a TLGG. One is called Lagrangian method which is based on a q-method developed by Von Neumann-Rithmyer[2]. Introducing an artificial viscosity into the pressure term in conservation equations, it can deal with the discontinuity at a shock in the flowfield and is suitable for shock-compression guns with a light piston. Another method to analyze two-stage gun problems is characteristics[3]. It has the advantage of less numerical error and more reliable computational results. But how to use this method to treat a flow with real gas effect, friction and heat transfer, and how to handle the transition and reflection of pressure

waves on transition sections between reservoir and pump tube and pump tube and barrel still remain open. In addition, a large number of variables in gun geometry and loading conditions made it an exceedingly ambiguous task to study the gun performance through experiments. Therefore, a new method is in urgent need that can numerically integrate unsteady partial differential equations of motion and involves the real gas effect, friction and heat transfer to meet the practical needs of the gun shooting under the conditions of high speed, high pressure and high temperature and miscellaneous environments.

In this paper, we put forward an appropriate way to deal with the propagation behavior of pressure waves across the transition section by using characteristic theory, and set up mathematical models to simulate the real gas effects, gas/wall and projectile/wall frictions and heat transfer. The influence of the gun geometry and loading conditions on the gun performance is investigated. This study demonstrates that characteristic theory can be used to compute and optimize the performance of two-stage light gas guns.

1 Basic equations

1.1 Gas dynamic equations

The gas motion in a TLGG is three-dimensional, unsteady and compressible, and the gas in a TLGG during a shot may undergo the process of high speed, high pressure and high temperature, so the real gas effect, friction and heat transfer should be involved in the governing equation of motion.

In most cases, the lengths of the reservoir, the pump tube and the barrel of a TLGG are much larger than their diameters, so we can assume that all the flow properties are constants in each cross-section normal to the axis of the gun so as to simplify the situation to one-dimensional compressible unsteady flow. The gas motion is then governed by three partial differential equations for the conservation of mass, momentum and energy:

$$\begin{cases} \dfrac{\partial \rho}{\partial t} + \dfrac{1}{A}\dfrac{\partial(\rho A u)}{\partial x} = 0, \\ \dfrac{\partial u}{\partial t} + u\dfrac{\partial u}{\partial x} + \dfrac{1}{\rho}\dfrac{\partial p}{\partial x} + F = 0, \\ \dfrac{\mathrm{d}}{\mathrm{d}t}\left(C_v T + \dfrac{u^2}{2}\right) = q - u\dfrac{\partial p}{\partial x} - \dfrac{p}{A}\dfrac{\partial}{\partial x}(Au). \end{cases} \tag{1}$$

Eq. (1) needs additional auxiliary equations and special modelisations on friction force F, heat flux q and state equation of the gas to close the system.

1.1.1 The equation of state. In order to include the effects of high pressure and high temperature, we take van der Waals expression as the state equation of the gas

$$(p+\alpha p^2)\,(1/\rho-\beta)=RT. \tag{2}$$

As a consequence of (2), the sound speed of the gas will meet the following relation:

$$c^2=\frac{\gamma p/\rho-\alpha\rho+2\alpha\beta\rho^2}{1-\beta\rho}. \tag{3}$$

1.1.2 Gas friction. In the absence of reliable data on transient, compressible flow friction, the semi-empirical relation is used to describe the effect of gas friction[4]:

$$F=\frac{1}{2}\,\frac{f}{D}\,u|u|. \tag{4}$$

The friction factor f is calculated as follows for different flow regions (laminar, transient and turbulent):

$$f=\begin{cases}\dfrac{64}{Re}\left(1+\dfrac{\gamma-1}{2}R_cM^2\right)^{-1}, & 0<Re\leqslant 2\,000\\[2ex] 0.32\left(1+\dfrac{\gamma-1}{2}R_cM^2\right)^{-1}\left(\dfrac{Re}{2\,000}\right)^{.3187}, & 2\,000<Re\leqslant 4\,000\\[2ex] \left(1+\dfrac{\gamma+1}{2}R_cM^2\right)^{-1}\left[1.14-2\ln\left(\dfrac{21.25}{Re^{.9}}+\dfrac{\varepsilon}{D}\right)\right]^{-2}. & 4\,000<Re\end{cases} \tag{5}$$

Reynolds number Re and viscous coefficient μ are taken as the function of temperature via the following from:

$$Re=\rho uD/\mu, \qquad \mu=C_1T^{\frac{3}{2}}/(C_2+C_3/T+T^{C_4}). \tag{6}$$

ε/D, M and R_c in eq. (5) stand for the relative roughness, Mach number and recovery factor, and C_1, C_2, C_3, C_4 in eq. (6) are gas-dependent constants.

1.1.3 Heat exchange To describe the heat exchange, we should first establish a mathematical model of the interaction between gas and wall, and a model for heat propagation in the wall. So define an adiabatic temperature, T_{ad}, of the wall:

$$T_{ad}=T\left(1+\frac{\gamma+1}{2}R_cM^2\right). \tag{7}$$

The heat flux entering the gas from the barrel is then

$$\varphi=h(T_w-T_{ad}), \tag{8}$$

where T_w is temperature on the wall and h is the heat exchange coefficient. Thus the quantity of heat per unit time and unit volume of the heated gas is

$$q=\frac{\varphi\pi D\Delta x}{\Delta x\pi D^2/4}. \tag{9}$$

Combining eqs. (8) and (9) gives

$$q=\frac{4h}{D}(T_w-T_{ad}). \tag{10}$$

Using the Reynolds analogy between heat and momentum transfer, one obtains

$$h=\frac{f}{8}|u|C_pP_r^{-2/3}, \tag{11}$$

where f is the friction coefficient, ρ the density of the barrel material, C_p the specific heat of the barrel material and P_r the Prandtl number.

On the wall, the heat penetration depth δ is figured out by using the semi-infinite slab approximation for conduction:

$$\delta=\sqrt{\pi\kappa t/\rho C_p}\,. \tag{12}$$

The heat balance between incoming heat through the gas/wall boundary and energy stored in the wall gives

$$\int_0^t h[T_{ad}(t)-T_w(t,0)\pi D\Delta x\mathrm{d}t=\int_0^\delta \rho C_p\pi D\Delta x[T_w(t,y)-T_\infty]\mathrm{d}y. \tag{13}$$

Assuming a linear temperature distribution on the wall for a time step Δt_n, (13) becomes

$$h_n(T_{abn}-T_{wn})\Delta t_n+\rho C_p\frac{\delta_{n-1}}{2}(T_{wn-1}-T_\infty)=\rho C_p\frac{\delta_n}{2}(T_{wn}-T_\infty). \tag{14}$$

If T_{adn} is constant in each time step, combining eqs. (12)—(14), we obtain

$$\frac{(T_\infty-T_{ad})}{(T_w-T_{ad})}=1+\frac{2h\sqrt{t}}{\sqrt{\pi\rho C_p\kappa}}\,. \tag{15}$$

Eqs. (7), (10), (11) and (15) are the relations to reckon heat exchange.

1.2 Characteristic equations

As the characteristic theory described in this paper includes the real gas effect, frictions and heat transfer, we should deduce the relation along a fluid particle for the computation, apart from the characteristics in the state plan.

From eq. (1), we obtain

$$q+uF=\frac{\mathrm{d}}{\mathrm{d}t}(C_vT)+\frac{p}{\rho A}\frac{\partial}{\partial x}(Au). \tag{16}$$

With eq. (2), one gets

$$\frac{\mathrm{d}}{\mathrm{d}t}(C_vT)=\frac{1-\beta\rho}{(\gamma-1)\rho}\left[\frac{\partial p}{\partial t}+u\frac{\partial p}{\partial x}+\left(2\alpha\rho-\frac{p+\alpha\rho^2}{\rho(1-\beta\rho)}\right)\left(\frac{\partial\rho}{\partial t}+u\frac{\partial\rho}{\partial x}\right)\right]. \tag{17}$$

Substitution of eq. (17) into eq. (16) yields, after rearrangement,

$$q+uF=\frac{1-\beta\rho}{(\gamma-1)\rho}\left[\frac{\partial p}{\partial t}+u\frac{\partial p}{\partial x}-c^2\left(\frac{\partial\rho}{\partial t}+u\frac{\partial\rho}{\partial x}\right)\right]. \tag{18}$$

Inserting the thermodynamics relation $Tds=\mathrm{d}(C_vT)+p\mathrm{d}(1/\rho)$ into (2), we find

$$T\mathrm{d}S=\frac{1-\beta\rho}{(\gamma-1)\rho}(\mathrm{d}p-c^2\mathrm{d}\rho). \tag{19}$$

Following a fluid particle there exists the relation:

$$\mathrm{d}p=\left(\frac{\partial p}{\partial t}+u\frac{\partial p}{\partial x}\right)\mathrm{d}t,\quad \mathrm{d}\rho=\left(\frac{\partial \rho}{\partial t}+u\frac{\partial \rho}{\partial x}\right)\mathrm{d}t. \tag{20}$$

Substituting (19), (20) into (18), we get

$$(\mathrm{d}S)_{\mathrm{path}}=\frac{q+uF}{T}(\mathrm{d}t)_{\mathrm{path}}. \tag{21}$$

The pressure may be taken as the function of sound speed and entropy:

$$\mathrm{d}p=\left(\frac{\partial p}{\partial c}\right)_s\mathrm{d}c+\left(\frac{\partial p}{\partial s}\right)_c\mathrm{d}S. \tag{22}$$

Obviously

$$\left(\frac{\partial p}{\partial c}\right)_s=\frac{2\gamma}{\gamma-1}\frac{p}{c},\quad \left(\frac{\partial p}{\partial s}\right)_c=-\rho T. \tag{23}$$

Combining these with (21) and (22), we obtain the characteristic equation along the flow path:

$$(\mathrm{d}p)_{\mathrm{path}}=\frac{2\gamma}{\gamma-1}\frac{p}{c}(\mathrm{d}c)_{\mathrm{path}}-\rho(q+uF)(\mathrm{d}t)_{\mathrm{path}}. \tag{24}$$

Based on the characteristic theory and (1), (22), characteristic equations in physical plane can be deduced:

$$\begin{cases}\left(\dfrac{\mathrm{d}x}{\mathrm{d}t}\right)_{1,2}=u\pm c, & \text{(Mach lines)}\\ \left(\dfrac{\mathrm{d}x}{\mathrm{d}t}\right)=u, & \text{(Path lines)}\end{cases} \tag{25}$$

and the characteristic equation in state plane:

$$(\mathrm{d}u)_{1,2}=\mp\frac{(\mathrm{d}p)_{1,2}}{\rho c}\mp\frac{cu}{A}\frac{\mathrm{d}A}{\mathrm{d}x}(\mathrm{d}t)_{1,2}\mp\frac{\gamma-1}{1-\beta\rho}\frac{q}{c}(\mathrm{d}t)_{1,2}-F\left(1\mp\frac{\gamma-1}{1-\beta\rho}\frac{u}{c}\right)(\mathrm{d}t)_{1,2}. \tag{26}$$

It is more convenient to work with the c, u-characteristics. To this end we have

$$\left(\frac{\mathrm{d}p}{\mathrm{d}t}\right)_{1,2}=\frac{\partial p}{\partial t}+\left(\frac{\mathrm{d}x}{\mathrm{d}t}\right)_{1,2},\quad \frac{\partial p}{\partial x}=\left(\frac{\mathrm{d}p}{\mathrm{d}t}\right)_{\mathrm{path}i}\pm c\frac{\partial p}{\partial x}. \tag{27}$$

In the same manner it may be shown that

$$\left(\frac{\mathrm{d}c}{\mathrm{d}t}\right)_{1,2}=\left(\frac{\mathrm{d}c}{\mathrm{d}t}\right)_{\mathrm{path}}\pm c\frac{\partial c}{\partial x}. \tag{28}$$

Insertion of this into eq.(26) yields the state characteristics in the form

$$(\mathrm{d}u)_{1,2}=\mp\frac{2}{\gamma-1}\left(1-\frac{\alpha-2\alpha\beta\rho-\beta c^2}{c^2}\right)(\mathrm{d}c)_{1,2}+\left[\mp\frac{cu}{A}\frac{\mathrm{d}A}{\mathrm{d}x}\mp\frac{\beta\rho}{1-\beta\rho}\frac{q+uF}{c}\right.$$

$$-F+\frac{p}{\rho}\frac{\partial}{\partial x}\left(\ln\frac{c^{2\gamma/(\gamma-1)}}{p}\right)\Bigg](\mathrm{d}t)_{1,2}. \tag{29}$$

1.3 Motion equations of piston and projectile

The basic factors determining the speed of the piston and projectile travelling in a two-stage gun may be simply obtained by applying Newton's force equation to them:

$$m_s\frac{\mathrm{d}u_s}{\mathrm{d}t}=A_s(p_s-p_{sf})-F_s,\quad m_b\frac{\mathrm{d}u_b}{\mathrm{d}t}=A_b(p_b-p_{bf})-F_b. \tag{30}$$

Since propellant pressures p_s, p_b and the counter pressure p_{sf}, p_{bf} and friction forces F_s, F_b are unknown, eq. (30) should be solved with eq. (29) simultaneously.

In the computation, the piston/wall friction F_s is ignored as the piston velocity is relatively low in a heavy piston gun.

The usual method to account for the projectile/wall friction F_b is to artificially use an increased projectile mass, or add a constant counterpressure in the motion equation. A more satisfatory mathematic model has now been implemented based on a large amount of experimental data.

To achieve this goal, let us first make the following basic assumptions:

(i) Friction forces vary in direct proportion to the normal stress.

(ii) Friction forces are (nearly) constant at low speeds then decreases with the increase of model velocity.

(iii) The friction shear stress cannot exceed the shear yield stress of the material.

These, together with the Von Mieses yield criterion, give the following formula for frictional shear stress τ_f:

$$\tau_f=\begin{cases}\mathrm{sign}(u)\nu\sigma_n, & |\nu\sigma_n|<\dfrac{\sigma_t}{\sqrt{3}},\\ -\mathrm{sign}(u)\dfrac{\sigma_t}{\sqrt{3}}, & |\nu\sigma_n|>\dfrac{\sigma_t}{\sqrt{3}}.\end{cases} \tag{31}$$

σ_n is the normal stress, σ_t the tensile yield strength and u the projectile speed.

The friction coefficient has the following form:

$$\nu=\begin{cases}\nu_s, & |u|\leqslant u_0,\\ \gamma_k+(\nu_s-\nu_k)\exp\left(-\dfrac{|u|-u_0}{u_d}\right), & |u|>u_0.\end{cases} \tag{32}$$

ν_s is the static friction coefficient, ν_k the dynamic friction coefficient, u_0 transition velocity and u_d the characteristic decay velocity.

Supposing a quasi-steady stress field in the projectile, and using Hook's Law for the

material stress/strain relation, the normal stress σ_n can be calculated in the following way:

$$\sigma_n = \frac{E(R_p - R_b)/R_b - \lambda p}{1-\lambda} . \tag{33}$$

E is the Young's elastic modules, λ the Poisson's coefficient, R_b the barrel inner radius, R_p the projectile unstressed radius, and p the local 1-D pressure field in the projectile.

The 1-D pressure field in the projectile can be determined from Newton's law of motion applied to the projectile assuming that all the points in the projectile move at the same speed:

$$\frac{dp}{dx} = \frac{2}{R_p}\tau_f - \rho\frac{du}{dt} . \tag{34}$$

Here ρ is the projectile density. Eq. (34) can be integrated analytically. When integrating eq. (34), one must be aware of whether a part of the projectile is in plastic deformation or not by the comparison between the projectile back pressure p_b and the elastic-plastic transition pressure p_e. From eq. (33), we find

$$p_e = \frac{\sigma_t}{\nu\sqrt{3}}\ \frac{1-\lambda}{\lambda} + \frac{E(R_p - R_b)}{\lambda R_b} . \tag{35}$$

In the elastic case where p_e is higher than back pressure p_b, we have the following value of the pressure field along the projectile:

$$p(x) = p_b\left(\frac{e^{\eta x} - e^{\eta l}}{1-e^{\eta l}}\right) + p_f\left(\frac{1-e^{\eta x}}{1-e^{\eta l}}\right), \tag{36}$$

where x is the axial location in the projectile, l the projectile length, and p_f the projectile front pressure, with $\eta = -2\gamma\lambda/R_p(1-\lambda)$.

In the elastic/plastic case, with $p_f \leqslant p_e \leqslant p_b$, the transition location x_e should be calculated first by an iterative process with the following formula:

$$x_e = \frac{p_b - p_e}{p_f - p_e}(1 - e^{\eta(l-x_e)})/\eta, \tag{37}$$

which enables us to compute the pressure in both elastic and plastic states

$$p(x) = \begin{cases} p_b - x(p_b - p_e)/x_e, & 0 \leqslant x \leqslant x_e, \\ p_f + (p_e - p_f)\dfrac{e^{\eta(x-l)} - 1}{e^{\eta(x_e - l)} - 1}, & x_e \leqslant x \leqslant l. \end{cases} \tag{38}$$

Eqs. (33)—(38) are the relations of computing the local frictional shear stress τ_f. Then integration over the projectile side surface gives the total friction force F on the projectile.

Back pressure p_{sf} is obtained from the flow field of the pump tube, and p_{bf} can be decided based on the initial pressure p_i in the barrel[3]:

$$P_{bf} = P_i\left\{1 + \frac{\gamma(\gamma+1)}{4}\left(\frac{u_b}{c}\right)^2 + \gamma\frac{u_b}{c}\left[1 + \left(\frac{\gamma+1}{4}\ \frac{u_b}{c}\right)^2\right]^{\frac{1}{2}}\right\}. \tag{39}$$

1.4 Linking conditions on the transition section

In a TLGG, the pump tube and the barrel of different cross-section areas are joined together by a short transition piece. For convenience, the flow in the transition may then, as an approximation, be treated as quasi-steady in character and replaced by a model in which there is a sudden change in cross-section. The flow across the transition section is linked by the conservation of mass, momentum and energy in quasi-steady state with isentropic assumption:

$$(\rho uA)_T=(\rho uA)_B,\ \left(\frac{c^2}{\gamma-1}+\frac{u^2}{2}\right)_T=\left(\frac{c^2}{\gamma-1}+\frac{u^2}{2}\right)_B. \tag{40}$$

The way to compute eq. (40) by characteristics is described in reference [6].

1.5 Initial and boundary conditions

In the case of $t=0$, $u=0$, $p=p_{or}$, $c=c_{or}$ (in the reservoir), $u=0$, $p=p_{op}$, $c=c_{op}$ (in the pump tube).

In the case of $t=t_{rd}$, $u=0$, $p=p_i$, $c=c_i$ (in the barrel).

Here t_{rd} presents the instant of time when the rupture disc is broken, p_{or}, p_{op}, p_i and c_{or}, c_{op}, c_i indicate the initial pressures and sound speeds in the reservoir, pump tube and barrel, respectively.

At the closed end of the reservoir, the gas remains standstill,

$$x=0,\ u=0 \text{ at all times.}$$

On the piston and the projectile, their velocities are equal to those of gases before and behind them,

$$u_s=u_{gas} \text{ and } u_b=u_{gas} \text{ at all times.}$$

2 Computational results

By using the characteristic theory described above, we have successfully programmed a numerical code to simulate the performance of a TLGG. In this section, we shall present some results obtained with this code and compare them with experimental data and comptational results by Lagrangian method[4].

The loading and geometry parameters for the results in the figures are listed in table 1.

Figure 1 gives a comparison of projectile speeds and projectile pressures along the barrel among the results from characteristics, Lagrangian method and experiment. The agreement is satisfactory between all three kinds of data. The consistence of projectile speeds seems even better. Projectile pressures are larger than the experimental in the former part of the barrel, and smaller in the latter part of the barrel.

Table 1 The gun geometry and loading conditions for the figures

Fig. No.	1	2	3	4	5	6	7
Res. /m×mm	0.7×80	0.7×80	0.7×80	0.7×80	0.7×80	0.7×80	1.5×100
P. T. /m×mm	3.0×80	3.0×80	3.0×80	3.0×80	3.0×80	3.0×80	5.0×100
Barrel/m×mm	1.5×6	1.5×6	1.5×6	1.5×6	1.5×6	1.5×6	2.5×6
Piston/kg	1.6	0.75	0.75	1.6	2.2		10.0
Proje. /mg	135	135	135	135	135	135	150
P_{or}/Mpa	9.2	9.25		9.25	9.2	9.25	9.0
P_{op}/Mpa	0.09	0.13	0.13		0.12	0.09	0.04
P_i/Mpa	0.0	0.0	0.0	0.0	0.0	0.0	0.0
P_{rd}/Mpa	29.0	30.0	30.0	30.0		30.0	60.0

Subcripts: or, reservoir; op, pump tube; i, barrel; rd, rupture disc. Nitrogen was fitted in the reservoir; hydrogen was fitted in the pump tube; res., reservoir; P. T., pump tube; Proje, projectile.

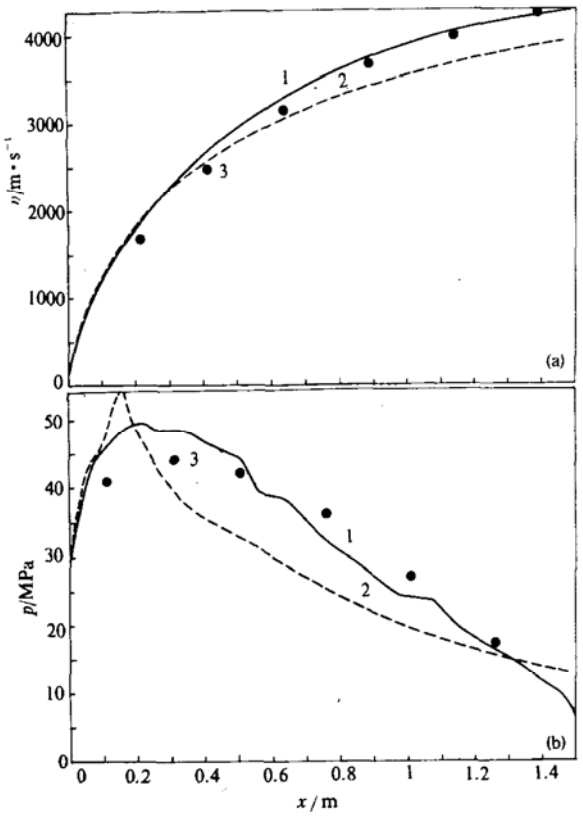

Fig. 1. Comparison between projectile speeds (a) and projecture pressures (b). 1. This paper; 2, ref. [4]; 3, experimental.

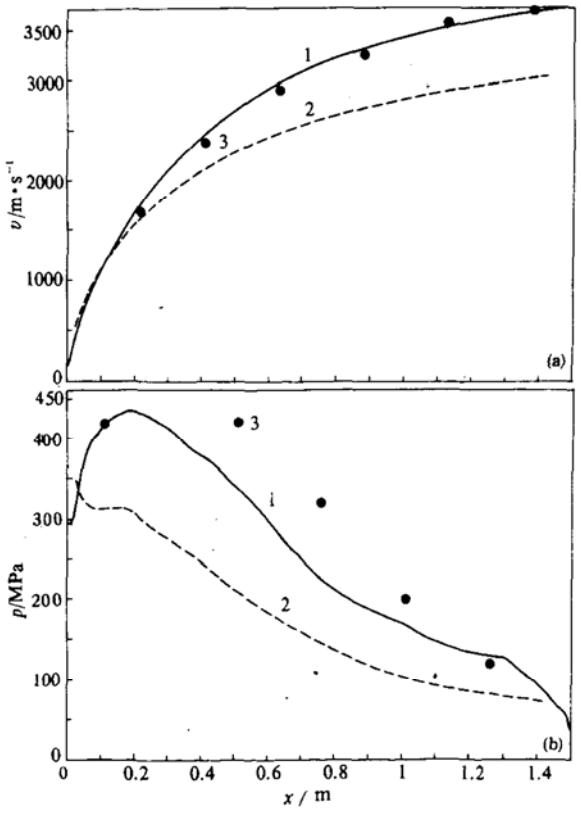

Fig. 2. Comparison between projectile speeds (a) and projectile pressures (b). 1, This paper; 2, ref. [4]; 3, experimental.

Figure 2 shows great difference in the two computations by given loading parameters. The values of projectile velicity and projectile pressure from Lagrangian method are smaller than those of characteristics.

Comparing experimental data, we find that the value obtained with characteristics are much closer to experimental ones. The comparisons suggest that the method given in this paper can well evaluate the performance of a TLGG.

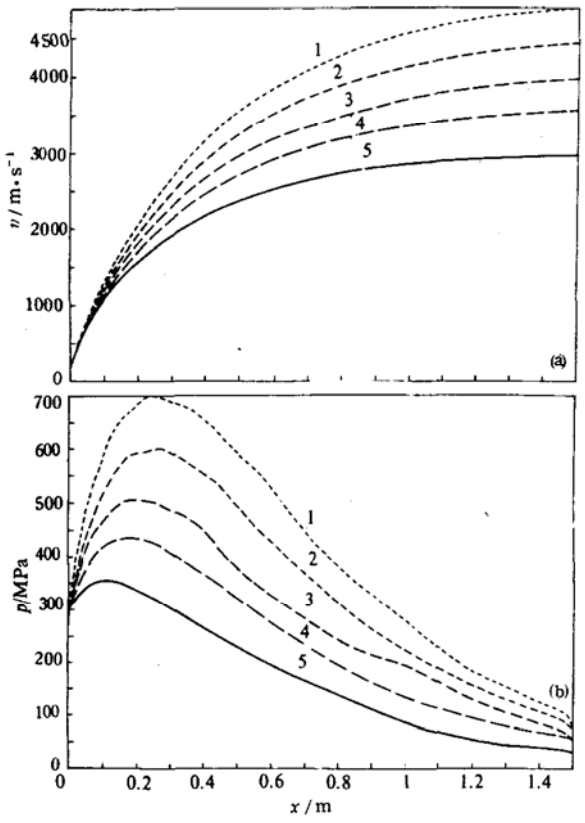

Fig. 3. Variation of speeds (a) and pressures (b) with p_{or}. 1, p_{or}=11 MPa; 2, p_{or}=10 MPa; 3, p_{or}=9 MPa; 4, p_{or}=8 MPa; 5, p_{or}=7 MPa.

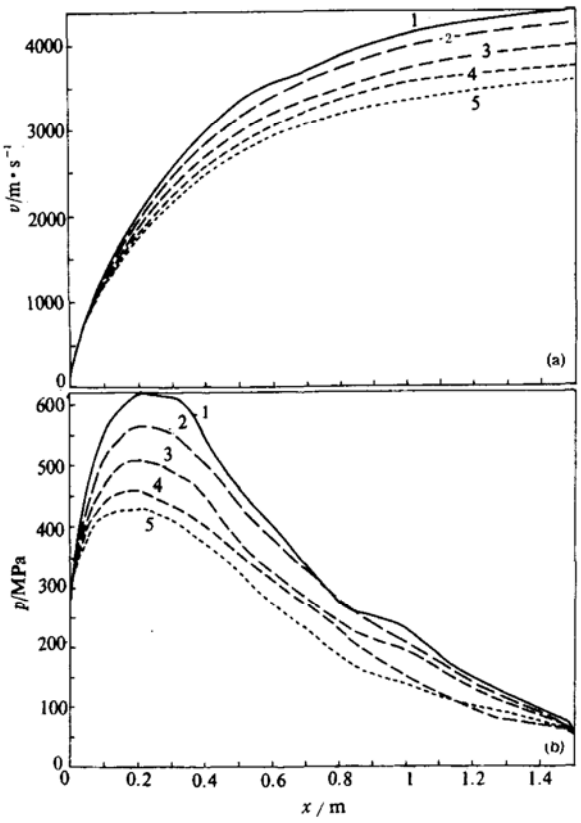

Fig. 4. Variation of speeds (a) and Pressure (b) with p_{op}. 1, p_{op}=0.11 MPa, 2, p_{op}=0.12 MPa, 3, p_{op}=0.13 MPa, 4, p_{op}=0.14 MPa; 5, p_{op}=0.15 MPa.

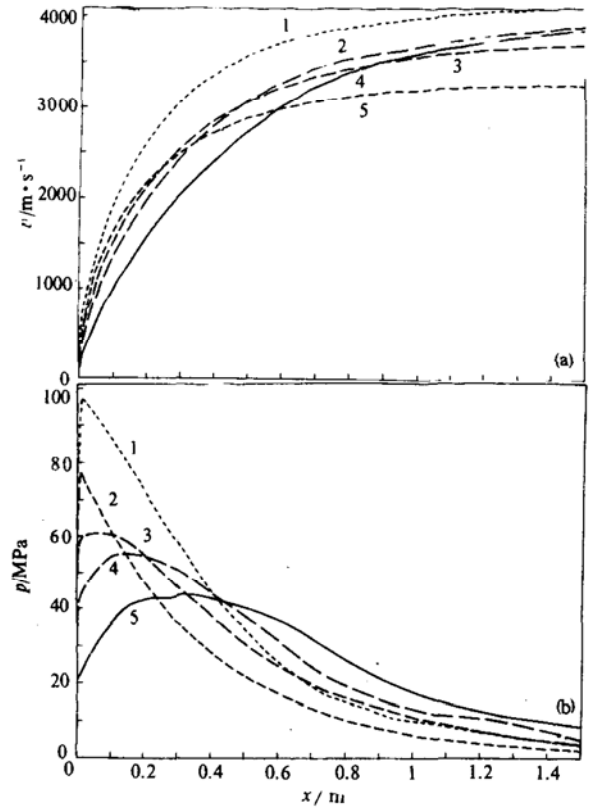

Fig. 5. Variation of speeds (a) and pressures (b) with p_{rd}. 1, p_{rd}=1 MPa; 2, p_{rd}=80 MPa; 3, p_{rd}=60 MPa; 4, p_{rd}=40 MPa; 5, p_{rd}=20 MPa.

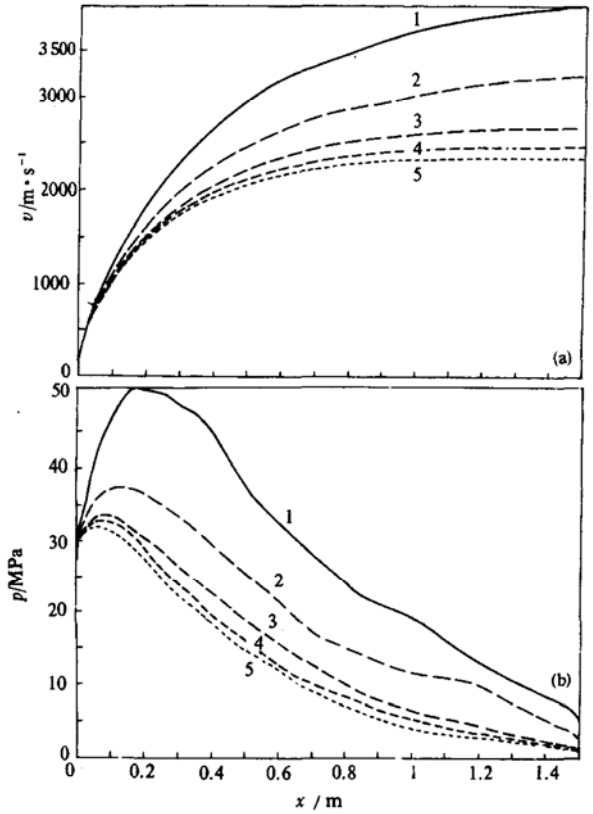

Fig. 6. Variation of speeds (a) and pressures (b) with M_S. 1, M_S=0.75 kg; 2, M_S=1.5 kg; 3, M_S=2.25 kg; 4, M_S=3 kg; 5, M_S=3.75 kg.

Figures 3—6 give the individual influence of loading parameters of p_{or}, p_{op}, p_{rd} and piston mass M_s.

As might have been expected, the projectile velocity and projectile pressure are directly proportional to the increase in p_{or} and inversely proportional to p_{op} (figs. 3 and 4). The location of peak pressure on the projectile moves slightly downwards with an increase in p_{or} and is almost unchanged with the variation in p_{op}.

The influence of p_{rd} is not so obvious as shown in fig. 5. For comparison, we choose $p_{rd}=20$, 40, 60, 80 or 100 MPa. When $p_{rd}=40$, the projectile velocity along the barrel is larger than when $p_{rd}=20$. But when $p_{rd}=60$, it drops down under the curves of $p_{rd}=20$ and 40 after the projectile moved some distance along the barrel; when $p_{rd}=80$, the decrease of projectile velocity is more significant; when p_{rd} increase to 100 MPa, it reaches the maximum. We can infer that with further increase in p_{rd}, it will increase.

Inspecting the distribution of projectile pressure in the figure, we find that the reason for this phenomenon is that with the increase in p_{rd}, the location of peak pressure on the projectile moves upwards in the barrel. This means that less and less compressive waves generated by the piston in the pump tube can catch up with the projectile, but the area covered by the pressure curve may still increase and result in a bigger projectile velocity; when p_{rd} increase to a certain extent, the area covered by the pressure curve will decrease rather than increase and a smaller velocity is generated. This process will continue until the location of peak pressure moves to the entrance of the barrel. From then on, no compressive waves can reach the projectile during its movement along the barrel. The performance of the gun is just like a one-stage gun without chambrage and the projectile velocity will increase with the increasing p_{rd}. This certainly does not encourage us to apply a bigger p_{rd} to gain a higher projectile muzzle velocity, because an intensive pressure and acceleration on the projectile at the very beginning of its movement will make it unstable or even destroy it. For a real shot, we not only hope that the projectile muzzle velocity will be as high as possible, but also require that the projectile move stable and in safety. Therefore, the choice of a proper p_{rd} in a real shot is very important for the gun performance.

Figure 6 shows the distribution of projectile speed and projectile pressure along the barrel for five different piston masses: 0.75, 1.5, 2.25, 3 and 3.75 kg. It seems that the lighter the piston mass, the higher the projectile speed and pressure. But we should note that the lighter the piston mass, the smaller the piston inertia and the shorter the pressure pulse in the pump tube. So a relatively light piston may be suitable for a moderate projectile muzzle velocity, but may not be helpful for achieving a very high projectile muzzle velocity.

Figure 7 points out that the real gas, friction and heat transfer do exert a distinguished influence on the gun performance. From the graph, we can see the losses reach 30% for

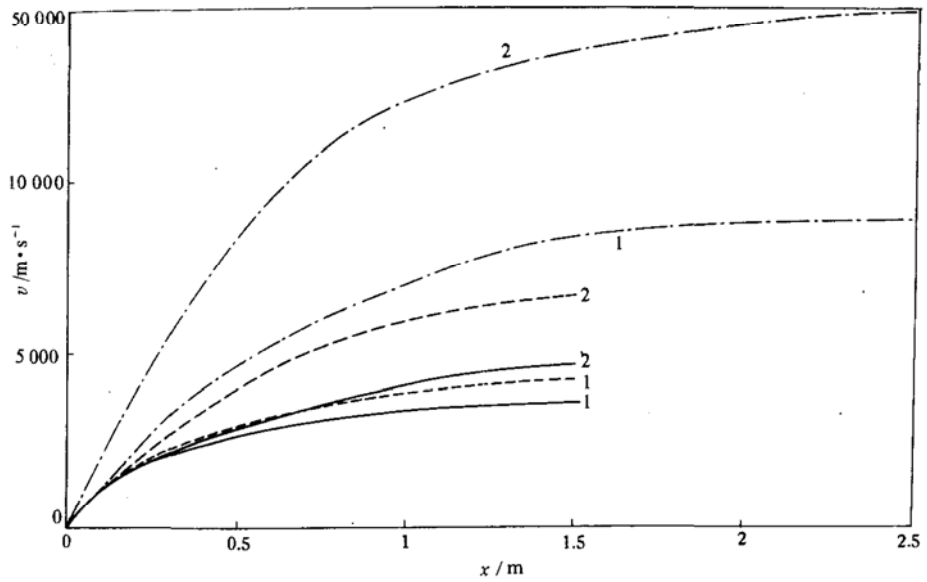

Fig. 7. Influences of real gas friction and heat transfer on gun performance. 1, Losses counted; 2, ideal circumstances.

real line case, 40% for dash line situation and as high as 70% for dash-dotted line circumstance. This indicates that the influence of real gas, friction and heat transfer can never be ignored when predicting the performance of a TLGG at high pressure, high temperature and high speed. The loading conditions and gun geometry for real line data and dash line are the same as those in figs. 1 and 2 (for dash-dotted line, refer to table 1).

3 Conclusions

A numerical model for characteristic formulation is put forward which has taken into account the real gas effect, friction and heat transfer. It is capable of simulating the actual process of a shot and enables us to obtain detailed information of various physical parameters. Comparisons of projectile velocities and projectile pressures along the barrel with experimental results show that this method can afford results with good accuracy over a wide range of gun geometry and loading conditions.

The mathematical models for simulating gas/wall heat transfer and projectile/wall friction are established and tested by numerical computations.

The choice of optimal combination of loading and shotting parameters especially the choice of rupture disc pressure p_{rd} is very important for optimizing the gun performance.

When predicting the performance of a TLGG at high temperature, high speed and high pressure, one must take into account the real gas effect, friction and heat transfer losses.

References

1 Canning, C. N., *AGARDograph*, 1970, 138.

2 Hardy, R. D., A program to predict performakce of a gas gun, *Sandia Laboratory Report Sand* 75-0323, New Mexico: Albuquerue, 1981.
3 Seigel, A. E., *AGARDograph* 91, 1965.
4 Flory, D., A code for the simulation of a two-stage gun for high speed pellet injection, *JET Joint Undertaking Report*, 1991.
5 Shapiro, A. H., *The Dynamics and Thermodynamics of Compressible Fluid Flow*, New York: The Ronald Press Co., 1953.
6 Wu Yingxiang, Zheng Zhichu, Lin Tongji, *Acta Armamentarii*, 1993, 4.